hep-ex/0607099

BABAR-CONF-06/034
SLAC-PUB-12025
July 2006

Measurement of the Branching Fractions for the Decays $B^+ \to \rho^+\gamma$, $B^0 \to \rho^0\gamma$, and $B^0 \to \omega\gamma$

The *BABAR* Collaboration

July 28, 2006

Abstract

We present preliminary results of a search for the decays $B^+ \to \rho^+\gamma$, $B^0 \to \rho^0\gamma$, and $B^0 \to \omega\gamma$. The analysis is based on data containing 347 million $B\overline{B}$ events recorded with the *BABAR* detector at the PEP-II B factory. We measure branching fractions of $\mathcal{B}(B^+ \to \rho^+\gamma) = (1.06^{+0.35}_{-0.31} \pm 0.09) \times 10^{-6}$ and $\mathcal{B}(B^0 \to \rho^0\gamma) = (0.77^{+0.21}_{-0.19} \pm 0.07) \times 10^{-6}$, where the first errors are statistical and the second systematic, and set a 90% C.L. upper limit of $\mathcal{B}(B^0 \to \omega\gamma) < 0.84 \times 10^{-6}$. Assuming isospin relations between the three branching fractions, these results are used to determine the CKM matrix element ratio $|V_{td}/V_{ts}| = 0.171^{+0.018}_{-0.021}(\text{exp.})^{+0.017}_{-0.014}(\text{theor.})$.

Submitted to the 33rd International Conference on High-Energy Physics, ICHEP 06,
26 July—2 August 2006, Moscow, Russia.

Stanford Linear Accelerator Center, Stanford University, Stanford, CA 94309

Work supported in part by US Department of Energy contract DE-AC02-76SF00515

The *BABAR* Collaboration,

B. Aubert, R. Barate, M. Bona, D. Boutigny, F. Couderc, Y. Karyotakis, J. P. Lees, V. Poireau, V. Tisserand, A. Zghiche

Laboratoire de Physique des Particules, IN2P3/CNRS et Université de Savoie, F-74941 Annecy-Le-Vieux, France

E. Grauges

Universitat de Barcelona, Facultat de Fisica, Departament ECM, E-08028 Barcelona, Spain

L. Lopez, A. Palano

Università di Bari, Dipartimento di Fisica and INFN, I-70126 Bari, Italy

J. C. Chen, N. D. Qi, G. Rong, P. Wang, Y. S. Zhu

Institute of High Energy Physics, Beijing 100039, China

G. Eigen, I. Ofte, B. Stugu

University of Bergen, Institute of Physics, N-5007 Bergen, Norway

G. S. Abrams, M. Battaglia, D. N. Brown, J. Button-Shafer, R. N. Cahn, E. Charles, M. S. Gill, Y. Groysman, R. G. Jacobsen, J. A. Kadyk, L. T. Kerth, Yu. G. Kolomensky, G. Kukartsev, G. Lynch, L. M. Mir, T. J. Orimoto, M. Pripstein, N. A. Roe, M. T. Ronan, W. A. Wenzel

Lawrence Berkeley National Laboratory and University of California, Berkeley, California 94720, USA

P. del Amo Sanchez, M. Barrett, K. E. Ford, A. J. Hart, T. J. Harrison, C. M. Hawkes, S. E. Morgan, A. T. Watson

University of Birmingham, Birmingham, B15 2TT, United Kingdom

T. Held, H. Koch, B. Lewandowski, M. Pelizaeus, K. Peters, T. Schroeder, M. Steinke

Ruhr Universität Bochum, Institut für Experimentalphysik 1, D-44780 Bochum, Germany

J. T. Boyd, J. P. Burke, W. N. Cottingham, D. Walker

University of Bristol, Bristol BS8 1TL, United Kingdom

D. J. Asgeirsson, T. Cuhadar-Donszelmann, B. G. Fulsom, C. Hearty, N. S. Knecht, T. S. Mattison, J. A. McKenna

University of British Columbia, Vancouver, British Columbia, Canada V6T 1Z1

A. Khan, P. Kyberd, M. Saleem, D. J. Sherwood, L. Teodorescu

Brunel University, Uxbridge, Middlesex UB8 3PH, United Kingdom

V. E. Blinov, A. D. Bukin, V. P. Druzhinin, V. B. Golubev, A. P. Onuchin, S. I. Serednyakov, Yu. I. Skovpen, E. P. Solodov, K. Yu Todyshev

Budker Institute of Nuclear Physics, Novosibirsk 630090, Russia

D. S. Best, M. Bondioli, M. Bruinsma, M. Chao, S. Curry, I. Eschrich, D. Kirkby, A. J. Lankford, P. Lund, M. Mandelkern, R. K. Mommsen, W. Roethel, D. P. Stoker

University of California at Irvine, Irvine, California 92697, USA

S. Abachi, C. Buchanan

University of California at Los Angeles, Los Angeles, California 90024, USA

S. D. Foulkes, J. W. Gary, O. Long, B. C. Shen, K. Wang, L. Zhang
University of California at Riverside, Riverside, California 92521, USA

H. K. Hadavand, E. J. Hill, H. P. Paar, S. Rahatlou, V. Sharma
University of California at San Diego, La Jolla, California 92093, USA

J. W. Berryhill, C. Campagnari, A. Cunha, B. Dahmes, T. M. Hong, D. Kovalskyi, J. D. Richman
University of California at Santa Barbara, Santa Barbara, California 93106, USA

T. W. Beck, A. M. Eisner, C. J. Flacco, C. A. Heusch, J. Kroseberg, W. S. Lockman, G. Nesom, T. Schalk, B. A. Schumm, A. Seiden, P. Spradlin, D. C. Williams, M. G. Wilson
University of California at Santa Cruz, Institute for Particle Physics, Santa Cruz, California 95064, USA

J. Albert, E. Chen, A. Dvoretskii, F. Fang, D. G. Hitlin, I. Narsky, T. Piatenko, F. C. Porter, A. Ryd, A. Samuel
California Institute of Technology, Pasadena, California 91125, USA

G. Mancinelli, B. T. Meadows, K. Mishra, M. D. Sokoloff
University of Cincinnati, Cincinnati, Ohio 45221, USA

F. Blanc, P. C. Bloom, S. Chen, W. T. Ford, J. F. Hirschauer, A. Kreisel, M. Nagel, U. Nauenberg, A. Olivas, W. O. Ruddick, J. G. Smith, K. A. Ulmer, S. R. Wagner, J. Zhang
University of Colorado, Boulder, Colorado 80309, USA

A. Chen, E. A. Eckhart, A. Soffer, W. H. Toki, R. J. Wilson, F. Winklmeier, Q. Zeng
Colorado State University, Fort Collins, Colorado 80523, USA

D. D. Altenburg, E. Feltresi, A. Hauke, H. Jasper, J. Merkel, A. Petzold, B. Spaan
Universität Dortmund, Institut für Physik, D-44221 Dortmund, Germany

T. Brandt, V. Klose, H. M. Lacker, W. F. Mader, R. Nogowski, J. Schubert, K. R. Schubert, R. Schwierz, J. E. Sundermann, A. Volk
Technische Universität Dresden, Institut für Kern- und Teilchenphysik, D-01062 Dresden, Germany

D. Bernard, G. R. Bonneaud, E. Latour, Ch. Thiebaux, M. Verderi
Laboratoire Leprince-Ringuet, CNRS/IN2P3, Ecole Polytechnique, F-91128 Palaiseau, France

P. J. Clark, W. Gradl, F. Muheim, S. Playfer, A. I. Robertson, Y. Xie
University of Edinburgh, Edinburgh EH9 3JZ, United Kingdom

M. Andreotti, D. Bettoni, C. Bozzi, R. Calabrese, G. Cibinetto, E. Luppi, M. Negrini, A. Petrella, L. Piemontese, E. Prencipe
Università di Ferrara, Dipartimento di Fisica and INFN, I-44100 Ferrara, Italy

F. Anulli, R. Baldini-Ferroli, A. Calcaterra, R. de Sangro, G. Finocchiaro, S. Pacetti, P. Patteri, I. M. Peruzzi,[1] M. Piccolo, M. Rama, A. Zallo
Laboratori Nazionali di Frascati dell'INFN, I-00044 Frascati, Italy

[1]Also with Università di Perugia, Dipartimento di Fisica, Perugia, Italy

A. Buzzo, R. Capra, R. Contri, M. Lo Vetere, M. M. Macri, M. R. Monge, S. Passaggio, C. Patrignani, E. Robutti, A. Santroni, S. Tosi

Università di Genova, Dipartimento di Fisica and INFN, I-16146 Genova, Italy

G. Brandenburg, K. S. Chaisanguanthum, M. Morii, J. Wu

Harvard University, Cambridge, Massachusetts 02138, USA

R. S. Dubitzky, J. Marks, S. Schenk, U. Uwer

Universität Heidelberg, Physikalisches Institut, Philosophenweg 12, D-69120 Heidelberg, Germany

D. J. Bard, W. Bhimji, D. A. Bowerman, P. D. Dauncey, U. Egede, R. L. Flack, J. A. Nash, M. B. Nikolich, W. Panduro Vazquez

Imperial College London, London, SW7 2AZ, United Kingdom

P. K. Behera, X. Chai, M. J. Charles, U. Mallik, N. T. Meyer, V. Ziegler

University of Iowa, Iowa City, Iowa 52242, USA

J. Cochran, H. B. Crawley, L. Dong, V. Eyges, W. T. Meyer, S. Prell, E. I. Rosenberg, A. E. Rubin

Iowa State University, Ames, Iowa 50011-3160, USA

A. V. Gritsan

Johns Hopkins University, Baltimore, Maryland 21218, USA

A. G. Denig, M. Fritsch, G. Schott

Universität Karlsruhe, Institut für Experimentelle Kernphysik, D-76021 Karlsruhe, Germany

N. Arnaud, M. Davier, G. Grosdidier, A. Höcker, F. Le Diberder, V. Lepeltier, A. M. Lutz, A. Oyanguren, S. Pruvot, S. Rodier, P. Roudeau, M. H. Schune, A. Stocchi, W. F. Wang, G. Wormser

Laboratoire de l'Accélérateur Linéaire, IN2P3/CNRS et Université Paris-Sud 11, Centre Scientifique d'Orsay, B.P. 34, F-91898 ORSAY Cedex, France

C. H. Cheng, D. J. Lange, D. M. Wright

Lawrence Livermore National Laboratory, Livermore, California 94550, USA

C. A. Chavez, I. J. Forster, J. R. Fry, E. Gabathuler, R. Gamet, K. A. George, D. E. Hutchcroft, D. J. Payne, K. C. Schofield, C. Touramanis

University of Liverpool, Liverpool L69 7ZE, United Kingdom

A. J. Bevan, F. Di Lodovico, W. Menges, R. Sacco

Queen Mary, University of London, E1 4NS, United Kingdom

G. Cowan, H. U. Flaecher, D. A. Hopkins, P. S. Jackson, T. R. McMahon, S. Ricciardi, F. Salvatore, A. C. Wren

University of London, Royal Holloway and Bedford New College, Egham, Surrey TW20 0EX, United Kingdom

D. N. Brown, C. L. Davis

University of Louisville, Louisville, Kentucky 40292, USA

J. Allison, N. R. Barlow, R. J. Barlow, Y. M. Chia, C. L. Edgar, G. D. Lafferty, M. T. Naisbit, J. C. Williams, J. I. Yi

University of Manchester, Manchester M13 9PL, United Kingdom

C. Chen, W. D. Hulsbergen, A. Jawahery, C. K. Lae, D. A. Roberts, G. Simi

University of Maryland, College Park, Maryland 20742, USA

G. Blaylock, C. Dallapiccola, S. S. Hertzbach, X. Li, T. B. Moore, S. Saremi, H. Staengle

University of Massachusetts, Amherst, Massachusetts 01003, USA

R. Cowan, K. Koeneke, M. I. Lang, G. Sciolla, S. J. Sekula, M. Spitznagel, F. Taylor, R. K. Yamamoto, M. Yi

Massachusetts Institute of Technology, Laboratory for Nuclear Science, Cambridge, Massachusetts 02139, USA

H. Kim, S. E. Mclachlin, P. M. Patel, S. H. Robertson

McGill University, Montréal, Québec, Canada H3A 2T8

A. Lazzaro, V. Lombardo, F. Palombo

Università di Milano, Dipartimento di Fisica and INFN, I-20133 Milano, Italy

J. M. Bauer, L. Cremaldi, V. Eschenburg, R. Godang, R. Kroeger, D. A. Sanders, D. J. Summers, H. W. Zhao

University of Mississippi, University, Mississippi 38677, USA

S. Brunet, D. Côté, M. Simard, P. Taras, F. B. Viaud

Université de Montréal, Physique des Particules, Montréal, Québec, Canada H3C 3J7

H. Nicholson

Mount Holyoke College, South Hadley, Massachusetts 01075, USA

N. Cavallo,[2] G. De Nardo, F. Fabozzi,[3] C. Gatto, L. Lista, D. Monorchio, P. Paolucci, D. Piccolo, C. Sciacca

Università di Napoli Federico II, Dipartimento di Scienze Fisiche and INFN, I-80126, Napoli, Italy

M. A. Baak, G. Raven, H. L. Snoek

NIKHEF, National Institute for Nuclear Physics and High Energy Physics, NL-1009 DB Amsterdam, The Netherlands

C. P. Jessop, J. M. LoSecco

University of Notre Dame, Notre Dame, Indiana 46556, USA

T. Allmendinger, G. Benelli, L. A. Corwin, K. K. Gan, K. Honscheid, D. Hufnagel, P. D. Jackson, H. Kagan, R. Kass, A. M. Rahimi, J. J. Regensburger, R. Ter-Antonyan, Q. K. Wong

Ohio State University, Columbus, Ohio 43210, USA

N. L. Blount, J. Brau, R. Frey, O. Igonkina, J. A. Kolb, M. Lu, R. Rahmat, N. B. Sinev, D. Strom, J. Strube, E. Torrence

University of Oregon, Eugene, Oregon 97403, USA

[2]Also with Università della Basilicata, Potenza, Italy
[3]Also with Università della Basilicata, Potenza, Italy

A. Gaz, M. Margoni, M. Morandin, A. Pompili, M. Posocco, M. Rotondo, F. Simonetto, R. Stroili, C. Voci
Università di Padova, Dipartimento di Fisica and INFN, I-35131 Padova, Italy

M. Benayoun, H. Briand, J. Chauveau, P. David, L. Del Buono, Ch. de la Vaissière, O. Hamon, B. L. Hartfiel, M. J. J. John, Ph. Leruste, J. Malclès, J. Ocariz, L. Roos, G. Therin
Laboratoire de Physique Nucléaire et de Hautes Energies, IN2P3/CNRS, Université Pierre et Marie Curie-Paris6, Université Denis Diderot-Paris7, F-75252 Paris, France

L. Gladney, J. Panetta
University of Pennsylvania, Philadelphia, Pennsylvania 19104, USA

M. Biasini, R. Covarelli
Università di Perugia, Dipartimento di Fisica and INFN, I-06100 Perugia, Italy

C. Angelini, G. Batignani, S. Bettarini, F. Bucci, G. Calderini, M. Carpinelli, R. Cenci, F. Forti, M. A. Giorgi, A. Lusiani, G. Marchiori, M. A. Mazur, M. Morganti, N. Neri, E. Paoloni, G. Rizzo, J. J. Walsh
Università di Pisa, Dipartimento di Fisica, Scuola Normale Superiore and INFN, I-56127 Pisa, Italy

M. Haire, D. Judd, D. E. Wagoner
Prairie View A&M University, Prairie View, Texas 77446, USA

J. Biesiada, N. Danielson, P. Elmer, Y. P. Lau, C. Lu, J. Olsen, A. J. S. Smith, A. V. Telnov
Princeton University, Princeton, New Jersey 08544, USA

F. Bellini, G. Cavoto, A. D'Orazio, D. del Re, E. Di Marco, R. Faccini, F. Ferrarotto, F. Ferroni, M. Gaspero, L. Li Gioi, M. A. Mazzoni, S. Morganti, G. Piredda, F. Polci, F. Safai Tehrani, C. Voena
Università di Roma La Sapienza, Dipartimento di Fisica and INFN, I-00185 Roma, Italy

M. Ebert, H. Schröder, R. Waldi
Universität Rostock, D-18051 Rostock, Germany

T. Adye, N. De Groot, B. Franek, E. O. Olaiya, F. F. Wilson
Rutherford Appleton Laboratory, Chilton, Didcot, Oxon, OX11 0QX, United Kingdom

R. Aleksan, S. Emery, A. Gaidot, S. F. Ganzhur, G. Hamel de Monchenault, W. Kozanecki, M. Legendre, G. Vasseur, Ch. Yèche, M. Zito
DSM/Dapnia, CEA/Saclay, F-91191 Gif-sur-Yvette, France

X. R. Chen, H. Liu, W. Park, M. V. Purohit, J. R. Wilson
University of South Carolina, Columbia, South Carolina 29208, USA

M. T. Allen, D. Aston, R. Bartoldus, P. Bechtle, N. Berger, R. Claus, J. P. Coleman, M. R. Convery, M. Cristinziani, J. C. Dingfelder, J. Dorfan, G. P. Dubois-Felsmann, D. Dujmic, W. Dunwoodie, R. C. Field, T. Glanzman, S. J. Gowdy, M. T. Graham, P. Grenier,[4] V. Halyo, C. Hast, T. Hryn'ova, W. R. Innes, M. H. Kelsey, P. Kim, D. W. G. S. Leith, S. Li, S. Luitz, V. Luth, H. L. Lynch, D. B. MacFarlane, H. Marsiske, R. Messner, D. R. Muller, C. P. O'Grady, V. E. Ozcan, A. Perazzo, M. Perl, T. Pulliam, B. N. Ratcliff, A. Roodman, A. A. Salnikov, R. H. Schindler, J. Schwiening, A. Snyder, J. Stelzer, D. Su, M. K. Sullivan, K. Suzuki, S. K. Swain, J. M. Thompson, J. Va'vra, N. van

[4]Also at Laboratoire de Physique Corpusculaire, Clermont-Ferrand, France

Bakel, M. Weaver, A. J. R. Weinstein, W. J. Wisniewski, M. Wittgen, D. H. Wright, A. K. Yarritu, K. Yi, C. C. Young

Stanford Linear Accelerator Center, Stanford, California 94309, USA

P. R. Burchat, A. J. Edwards, S. A. Majewski, B. A. Petersen, C. Roat, L. Wilden

Stanford University, Stanford, California 94305-4060, USA

S. Ahmed, M. S. Alam, R. Bula, J. A. Ernst, V. Jain, B. Pan, M. A. Saeed, F. R. Wappler, S. B. Zain

State University of New York, Albany, New York 12222, USA

W. Bugg, M. Krishnamurthy, S. M. Spanier

University of Tennessee, Knoxville, Tennessee 37996, USA

R. Eckmann, J. L. Ritchie, A. Satpathy, C. J. Schilling, R. F. Schwitters

University of Texas at Austin, Austin, Texas 78712, USA

J. M. Izen, X. C. Lou, S. Ye

University of Texas at Dallas, Richardson, Texas 75083, USA

F. Bianchi, F. Gallo, D. Gamba

Università di Torino, Dipartimento di Fisica Sperimentale and INFN, I-10125 Torino, Italy

M. Bomben, L. Bosisio, C. Cartaro, F. Cossutti, G. Della Ricca, S. Dittongo, L. Lanceri, L. Vitale

Università di Trieste, Dipartimento di Fisica and INFN, I-34127 Trieste, Italy

V. Azzolini, N. Lopez-March, F. Martinez-Vidal

IFIC, Universitat de Valencia-CSIC, E-46071 Valencia, Spain

Sw. Banerjee, B. Bhuyan, C. M. Brown, D. Fortin, K. Hamano, R. Kowalewski, I. M. Nugent, J. M. Roney, R. J. Sobie

University of Victoria, Victoria, British Columbia, Canada V8W 3P6

J. J. Back, P. F. Harrison, T. E. Latham, G. B. Mohanty, M. Pappagallo

Department of Physics, University of Warwick, Coventry CV4 7AL, United Kingdom

H. R. Band, X. Chen, B. Cheng, S. Dasu, M. Datta, K. T. Flood, J. J. Hollar, P. E. Kutter, B. Mellado, A. Mihalyi, Y. Pan, M. Pierini, R. Prepost, S. L. Wu, Z. Yu

University of Wisconsin, Madison, Wisconsin 53706, USA

H. Neal

Yale University, New Haven, Connecticut 06511, USA

1 INTRODUCTION

In the Standard Model (SM) description of the decays[1] $B^+ \to \rho^+\gamma$, $B^0 \to \rho^0\gamma$, and $B^0 \to \omega\gamma$, the dominant contributions arise from $b \to d\gamma$ penguin diagrams of the type shown in Figure 1.

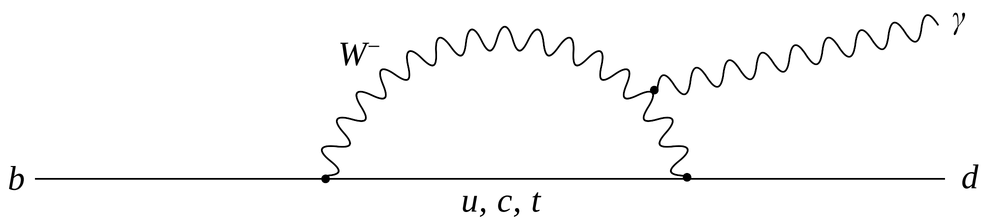

Figure 1: Feynman diagram for $b \to d\gamma$.

Relating the three individual decay rates by isospin symmetry and using the measured ratio between the charged and neutral B-meson lifetimes $\tau_{B^+}/\tau_{B^0} = 1.071 \pm 0.009$ [15], one can define a combined branching fraction

$$\overline{\mathcal{B}}[B \to (\rho/\omega)\gamma] \equiv \mathcal{B}(B^+ \to \rho^+\gamma) = 2\frac{\tau_{B^+}}{\tau_{B^0}}\mathcal{B}(B^0 \to \rho^0\gamma) = 2\frac{\tau_{B^+}}{\tau_{B^0}}\mathcal{B}(B^0 \to \omega\gamma) \quad (1)$$

The results of recent calculations of $\overline{\mathcal{B}}[B \to (\rho/\omega)\gamma]$ are in the range of $(0.9\text{–}1.8) \times 10^{-6}$ [1–3]; however, these could be modified by processes beyond the SM [4]. Within the SM, the isospin violation in these decays is expected to be small; a recent estimate [2] is $(1.1 \pm 3.9)\%$.

While the exclusive rates have a large uncertainty due to non-perturbative long-distance QCD effects, much of this uncertainty cancels in the ratio of $B \to (\rho/\omega)\gamma$ and $B \to K^*\gamma$ rates. Since the dominant diagram in Figure 1 involves a virtual top quark, this ratio is related to the ratio of Cabibbo-Kobayashi-Maskawa (CKM) matrix elements $|V_{td}/V_{ts}|$ [1, 2] via

$$\frac{\overline{\mathcal{B}}(B \to (\rho/\omega)\gamma)}{\mathcal{B}(B \to K^*\gamma)} = \left|\frac{V_{td}}{V_{ts}}\right|^2 \left(\frac{1 - m_\rho^2/M_B^2}{1 - m_{K^*}^2/M_B^2}\right)^3 \zeta^2[1 + \Delta R]. \quad (2)$$

Here, the form factor ratio ζ describes the flavor-SU(3) symmetry breaking between ρ/ω and K^*, and ΔR accounts for annihilation diagrams. Physics beyond the Standard Model could affect these decays and create inconsistencies between the measurements of $|V_{td}/V_{ts}|$ obtained from this analysis and those obtained in studies of B_s^0 and B_d^0 mixing.

Previous searches by *BABAR* [5] and CLEO [6] have found no evidence for $B \to (\rho/\omega)\gamma$ decays. An observation of the decay $B^0 \to \rho^0\gamma$ was recently reported by the Belle collaboration [7].

In this paper we report a search for the decays $B^+ \to \rho^+\gamma$, $B^0 \to \rho^0\gamma$, and $B^0 \to \omega\gamma$. The results presented in this paper use a *BABAR* data sample containing 347 million $B\overline{B}$ events, corresponding to an integrated luminosity of $316\,\text{fb}^{-1}$, and supersede those in Ref. [5].

[1]Charge conjugate modes are implicitly included throughout.

2 THE *BaBar* DETECTOR

The data used in this analysis were collected with the *BABAR* detector at the PEP-II asymmetric–energy e^+e^- storage ring. Charged particle trajectories are measured by a combination of a five-layer silicon vertex tracker and a 40-layer drift chamber in a 1.5-T magnetic field. Photons and electrons are detected in a CsI(Tl) crystal electromagnetic calorimeter (EMC) with photon energy resolution $\sigma_E/E = 0.023(E/\mathrm{GeV})^{-1/4} \oplus 0.019$. A ring-imaging Cherenkov detector (DIRC) is used for charged-particle identification. In order to identify muons, the magnetic flux return is instrumented with resistive plate chambers and limited streamer tubes. A detailed description of the detector can be found elsewhere [8].

3 EVENT RECONSTRUCTION AND SELECTION

The decays $B^+ \to \rho^+\gamma$, $B^0 \to \rho^0\gamma$, and $B^0 \to \omega\gamma$ are reconstructed by combining a high-energy photon with a vector meson exclusively reconstructed in the decays $\rho^0 \to \pi^+\pi^-$ ($\mathcal{B} \approx 100\%$), $\rho^+ \to \pi^+\pi^0$ ($\mathcal{B} \approx 100\%$), and $\omega \to \pi^+\pi^-\pi^0$ ($\mathcal{B} = [89.1 \pm 0.7]\%$ [15]).

The primary source of background is due to continuum events ($e^+e^- \to q\bar{q}$, with $q = u, d, s, c$) that contain a high-energy photon from π^0 or η decays or from initial-state radiation (ISR). Decays of $B \to K^*\gamma$, $K^* \to K\pi$ can enter the signal selection, e.g., when a $K^\pm$ is misidentified as a $\pi^\pm$. $B \to (\rho/\omega)\pi^0$ and $B \to (\rho/\omega)\eta$ processes are also found to be relevant when a high-energy photon is produced in the π^0 or η decay. In addition, there is combinatorial background from high-multiplicity $b \to s\gamma$ decays. These backgrounds are suppressed by applying the selection requirements described below. These requirements have been optimized separately for each signal mode, using simulated signal and background event samples and the method described in [9], for maximum statistical sensitivity[2] assuming a branching fraction of $1.0(0.5) \times 10^{-6}$ for the charged(neutral) mode.

The photon from the signal B decay is identified as a localized energy deposit (cluster) in the calorimeter with energy $1.5 < E^*_\gamma < 3.5$ GeV in the center-of-mass (CM) frame. The energy deposit must not be associated with any reconstructed charged track, be well-isolated from other EMC clusters, and meet a number of further requirements designed to eliminate background from hadronic showers, small-angle photon pairs, and charged particles [10].

We veto those photons that can be associated with another detected photon to form a π^0 or η candidate using the likelihood ratio

$$\frac{\mathcal{P}(M(\gamma\gamma'), E_{\gamma'}|i)}{\mathcal{P}(M(\gamma\gamma'), E_{\gamma'}|\mathrm{signal}) + \mathcal{P}(M(\gamma\gamma'), E_{\gamma'}|i)}, \quad i = \pi^0, \eta. \qquad (3)$$

In this definition, $\mathcal{P}$ is the probability density function defined in terms of the invariant mass of the photon pair, $M(\gamma\gamma')$, and the energy of γ' in the laboratory frame, $E_{\gamma'}$, as determined from simulated signal and background events. To consider photons coming from the decays of π^0 and η that have converted to e^+e^- pairs, we combine the high-energy photon candidate with any e^+e^- pair in the event with an invariant mass $m_{e^+e^-} < 50$ MeV/c^2, and reject the photon if the total invariant mass satisfies either $100 < m_{\gamma e^+e^-} < 160\,\mathrm{MeV}/c^2$ or $500 < m_{\gamma e^+e^-} < 590\,\mathrm{MeV}/c^2$.

Charged pion candidates are selected from well-reconstructed tracks with a minimum momentum transverse to the beam direction of 100 MeV/c. In order to reduce backgrounds from charged kaons produced in $b \to s\gamma$ processes, a $\pi^\pm$ selection algorithm [5] is applied, combining DIRC information with the energy loss measured in the tracking system.

[2]Here, the figure of merit is $S/\sqrt{(S+B)}$, where S and B are the rates for signal and backgrounds respectively.

Photon candidates identified in the EMC with energy greater than 50 MeV are combined into pairs to form π^0 candidates. For $B^0 \to \omega\gamma$ ($B^+ \to \rho^+\gamma$) decays, the invariant mass of the pair is required to satisfy $122 < m_{\gamma\gamma} < 150$ MeV/c^2 ($117 < m_{\gamma\gamma} < 148$ MeV/c^2). We also require the cosine of the opening angle between the daughter photons in the laboratory frame be greater than 0.413 and 0.789 for $B^0 \to \omega\gamma$ and $B^+ \to \rho^+\gamma$ respectively.

The identified pions are combined into vector meson candidates by requiring $633 < m_{\pi^+\pi^-} < 957$ MeV/c^2, $636 < m_{\pi^+\pi^0} < 932$ MeV/c^2, and $764 < m_{\pi^+\pi^-\pi^0} < 795$ MeV/c^2 for ρ^0, ρ^+, and ω respectively. The charged pion pair must originate from a common vertex, which is required to be consistent with the interaction region to suppress K^0_S decays.

The photon and ρ/ω candidates are combined to form the B-meson candidates. We define $\Delta E \equiv E^*_B - E^*_{\rm beam}$, where E^*_B is the CM energy of the B-meson candidate and $E^*_{\rm beam}$ is the CM beam energy. We also define the beam-energy-substituted mass $m_{\rm ES} \equiv \sqrt{E^{*2}_{\rm beam} - \vec{\rm p}^{*2}_B}$, where $\vec{\rm p}^*_B$ is the CM momentum of the B candidate. Signal events are expected to have a ΔE distribution centered at zero with a resolution of about 50 MeV, and a $m_{\rm ES}$ distribution centered at the mass of the B meson, m_B, with a resolution of 3 MeV/c^2. We consider candidates in the ranges $-0.3 < \Delta E < 0.3$ GeV and $m_{\rm ES} > 5.22$ GeV/c^2 to incorporate sidebands that allow the combinatorial background yields to be extracted from a fit to the data.

To suppress $B \to \rho(\pi^0/\eta)$ and $B \to \omega(\pi^0/\eta)$ events, we calculate the vector meson helicity angle, θ_H, defined as the angle between the π^- track (normal to the ω decay plane) and the B momentum vector in the ρ (ω) rest frame. We require $|\cos\theta_H| < 0.75$.

Contributions from continuum background processes are reduced by considering only events for which the ratio R_2 of second-to-zeroth order Fox-Wolfram moments [11] is less than 0.7. In addition, several variables that distinguish between signal and continuum events are combined in a neural network. The quantity R'_2, which is R_2 in the frame recoiling against the photon momentum, is used to reject ISR events. To discriminate between the jet-like continuum background and the more spherically-symmetric signal events, we compute the angle between the photon and the thrust axis of the rest of the event (ROE) in the CM frame. The ROE is defined by all the charged tracks and neutral energy deposits in the calorimeter that are not used to reconstruct the B candidate. We also calculate the moments $L_i \equiv \sum_j p^*_j \cdot |\cos\theta^*_j|^i / \sum_j p^*_j$, where p^*_j and θ^*_j are the momentum and angle with respect to an axis, respectively, for each particle j in the ROE. We use L_1, L_2, and L_3 with respect to the thrust axis of the ROE, as well as with respect to the photon direction. In addition, we calculate the B-meson production angle θ^*_B with respect to the beam axis in the CM frame. Differences in lepton and kaon production between background and B decays are exploited by including flavor-tagging variables [12] as well as the maximum CM momentum and number of $K^\pm$ and K^0_S in the ROE. The significance of the separation along the beam axis of the B-meson candidate and ROE vertices is included as well. To reject events for which this quantity is poorly reconstructed, the separation along the beam axis and the associated uncertainty are required to be less than 4 mm and 0.4 mm, respectively.

We train the neural network separately for each signal mode and select $B^+ \to \rho^+\gamma$, $B^0 \to \rho^0\gamma$, and $B^0 \to \omega\gamma$ candidates with a requirement on the the neural-network output that retains 63%, 74%, and 71% of the signal events respectively. For these cuts, we determine the continuum background efficiencies using a data sample of $27.2 fb^{-1}$ taken 40 MeV below the $\Upsilon(4S)$ resonance as 3.0%, 5.3% and 6.7% for the three signal modes respectively.

The expected average candidate multiplicity in the selected signal events is 1.01 for $B^0 \to \rho^0\gamma$ and 1.07 for $B^+ \to \rho^+\gamma$ and $B^0 \to \omega\gamma$; in events with multiple candidates the one with the reconstructed vector meson mass closest to the nominal mass is retained.

Applying all the selection criteria described above, we find efficiencies of 11.6% for $B^+ \to \rho^+\gamma$, 14.5% for $B^0 \to \rho^0\gamma$, and 8.1% for $B^0 \to \omega\gamma$.

4 MAXIMUM LIKELIHOOD FIT

The signal content of the data is determined by means of a multi-dimensional unbinned maximum likelihood fit, which is constructed individually for each of the three signal decay modes. All fits use ΔE, m_{ES} , $\cos\theta_H$, and the neural-network output NN, after transforming it according to

$$\mathcal{NN} = \tanh^{-1}\left(\frac{(NN - c_1)\cdot(1-c_2)}{c_3}\right), \quad c_i = \text{constant} \tag{4}$$

in order to facilitate the parameterization of the probability density function (PDF) used in the fit. For $B^0 \to \omega\gamma$, the cosine of the Dalitz angle θ_D [5] is added as a fifth observable.

In addition to signal and continuum background processes, we consider several sources of background from B decays, which in the fit are combined in different ways depending on the signal mode under study. In the $B^0 \to \omega\gamma$ fit, all B backgrounds are combined into a single component, while for the $B^0 \to \rho^0\gamma$ analysis $B^+ \to K^{*+}\gamma$, $B^0 \to K^{*0}\gamma$, and other B background processes are treated separately. The $B^+ \to \rho^+\gamma$ fit uses four different categories of B backgrounds: $B^+ \to K^{*+}\gamma$ with $K^{*+} \to K^+\pi^0$, other $B \to K^*\gamma$ decays, $B \to X_s\gamma$ processes (excluding $B \to K^*\gamma$), and remaining B backgrounds.

In studies of simulated signal and background event samples, the correlations among the observables are found to be small. We therefore assume that the PDF $\mathcal{P}(\vec{x_j};\vec{\alpha_i})$ for each of the N_{hyp} event hypotheses is the product of individual PDFs for the fit observables $\vec{x}_j$ given the set of parameters $\vec{\alpha}_i$. The likelihood function for signal mode k ($=\rho^+\gamma$, $\rho^0\gamma$, $\omega\gamma$) is defined as

$$\mathcal{L}_k = \exp\left(-\sum_{i=1}^{N_{\mathrm{hyp}}} n_i\right)\cdot\left[\prod_{j=1}^{N_k}\left(\sum_{i=1}^{N_{\mathrm{hyp}}} n_i\mathcal{P}_i(\vec{x}_j;\ \vec{\alpha}_i)\right)\right], \tag{5}$$

where n_i is the yield of each hypothesis and N_k is the number of candidate events observed in data.

The functional form of each PDF is determined from a one-dimensional fit to a dedicated sample of simulated events. The ΔE distribution is corrected for the observed difference between data and simulated samples of $B \to K^*\gamma$ decays. All continuum background PDF parameters float freely in the fits while the shapes of the signal and B background distributions are fixed. For $B^0 \to \omega\gamma$, the B background yield floats freely in the fit. In the $B^+ \to \rho^+\gamma$ analysis, the $B^+ \to K^{*+}\gamma$ ($K^{*+} \to K^+\pi^0$) contribution and the ratio of the other three B background yields are determined from simulated events, as are the relative contributions from the three B background components in the $B^0 \to \rho^0\gamma$ fit.

For the signal, the m_{ES} spectra are described by Crystal Ball functions [13], the angular distributions are modeled by second-order polynomials, and the distributions of ΔE and $\mathcal{NN}$ are parametrized as asymmetric, variable-width Gaussians

$$f(x) = \exp\left[\frac{-(x-\mu)^2}{2\sigma_{L,R}^2 + \alpha_{L,R}(x-\mu)^2}\right], \tag{6}$$

where μ is the peak position of the distribution, $\sigma_{L,R}$ are the width left and right of the peak, and $\alpha_{L,R}$ are a measure of the tail on the left and right side of the peak respectively.

The function (6) also describes the continuum background $\mathcal{NN}$ shape; the remaining continuum spectra are modeled by ARGUS functions [14] ($m_{\rm ES}$) or second- and fourth-order polynomials (ΔE, $\cos\theta_H$, and $\cos\theta_D$). Various functional forms are used to describe the different B background components.

In order to measure the combined branching fraction $\overline{\mathcal{B}}[B \to (\rho/\omega)\gamma]$, we also perform a simultaneous fit to the three decay–mode specific data sets for the effective signal yield $n_{\rm eff}$, which is related to signal yields and reconstruction efficiencies[3] obtained from the individual fits via $n(B^+ \to \rho^+\gamma) = n_{\rm eff} \cdot \frac{1}{2}\epsilon(B^+ \to \rho^+\gamma)$ and $n(B^0 \to (\rho^0/\omega)\gamma) = \frac{1}{4}\frac{\tau_{B^0}}{\tau_{B^+}} n_{\rm eff} \cdot \epsilon(B^0 \to (\rho^0/\omega)\gamma)$.

Figures 2, 3, and 4 show the projections of the fit results for $B^+ \to \rho^+\gamma$, $B^0 \to \rho^0\gamma$, and $B^0 \to \omega\gamma$ respectively compared to the data; for each plot the signal fraction is enhanced by selections on the other fit variables. The resulting signal yields are given in Table 2. The significance is computed as $\sqrt{2\Delta\log\mathcal{L}}$, where $\Delta\log\mathcal{L}$ is the log-likelihood difference between the best fit and a fit to the null-signal hypothesis; only statistical uncertainties are included here.

5 SYSTEMATIC UNCERTAINTIES

Table 1 gives an overview of the contributions to the systematic uncertainties. These are associated with the signal reconstruction efficiency, the modeling of $B\overline{B}$ backgrounds, and the choice of fixed parameters of the fit PDFs. The latter two contribute to the uncertainties on the signal yields. A small uncertainty on the overall normalization is associated with the imperfect knowledge of the total number of $B\overline{B}$ pairs in the underlying data sample.

Table 1: Fractional systematic errors (in %) of the measured branching fractions.

Source of error	$B^+ \to \rho^+\gamma$	$B^0 \to \rho^0\gamma$	$B^0 \to \omega\gamma$
Tracking efficiency	1.0%	2.0%	2.0%
Charged-particle identification	2.0%	4.0%	2.0%
Photon selection	1.9%	2.6%	1.7%
π^0 reconstruction	3.0%	-	3.0%
π^0 and η veto	2.8%	2.8%	2.8%
$\mathcal{NN}$ efficiency	5.0%	3.5%	3.5%
ΔE shape from $K^*\gamma$	3.1%	2.4%	1.9%
$\mathcal{NN}$ shape	0.2%	3.9%	4.7%
B background normalization	3.0%	4.0%	-
B counting	1.1%	1.1%	1.1%
Combined	8.4%	9.2%	8.2%

The signal efficiency systematic error includes uncertainties from tracking, charged-particle

[3] The efficiencies include the daughter branching fractions.

Table 2: The signal yield ($n_{\rm sig}$), statistical significance in standard deviations (σ), efficiency (ϵ), and branching fraction ($\mathcal{B}$) central value for each mode. The errors on ($n_{\rm sig}$) are statistical only, while for the branching fraction the first errors are statistical and the second systematic. All results are preliminary.

Mode	$n_{\rm sig}$	Significance	$\epsilon(\%)$	$\mathcal{B}(10^{-6})$	
$B^+ \to \rho^+\gamma$	$42.4^{+14.1}_{-12.6}$	4.1σ	11.6	$1.06^{+0.35}_{-0.31} \pm 0.09$	
$B^0 \to \rho^0\gamma$	$38.7^{+10.6}_{-9.8}$	5.2σ	14.5	$0.77^{+0.21}_{-0.19} \pm 0.07$	
$B^0 \to \omega\gamma$	$11.0^{+6.7}_{-5.6}$	2.3σ	8.1	$0.39^{+0.24}_{-0.20} \pm 0.03$	(< 0.84 at 90% C.L.)

identification, γ/π^0 reconstruction, photon selection and the neural network selection that are determined from suitable independent data control samples.

To estimate the uncertainty related to the extraction of the signal PDFs from MC distributions, we vary the parameters within their errors. The uncertainty related to the choice of a specific functional form for the shape of the $\mathcal{NN}$ distributions is evaluated by using a binned histogram as an alternative PDF. All relative and absolute normalizations of B background components which were fixed in the fit are varied by 50%. For all these variations, the corresponding change in the fitted signal yield is taken as a systematic uncertainty.

6 RESULTS

The branching fractions are calculated from the fitted signal yields assuming $\mathcal{B}(\Upsilon(4S) \to B^0\overline{B}^0) = \mathcal{B}(\Upsilon(4S) \to B^+B^-) = 0.5$. For $B^0 \to \omega\gamma$, we also compute the corresponding 90% confidence level (C.L.) upper limit using a Bayesian technique. The signal yield upper limit n_l is determined such that $\int_0^{n_l} \mathcal{L}\,dn / \int_0^{\infty} \mathcal{L}\,dn = 0.90$, assuming a flat prior. The systematic uncertainty is included by increasing n_l and decreasing the detection efficiency by their respective errors. The results are listed in Table 2.

The simultaneous fit finds an effective signal yield $n_{\rm eff} = 702^{+150}_{-141}$ with a corresponding statistical significance of 6.3 σ. This translates into a combined branching fraction

$$\overline{\mathcal{B}}[B \to (\rho/\omega)\gamma] = (1.01 \pm 0.21 \pm 0.08) \times 10^{-6}. \quad (7)$$

We also measure the ratio $\Gamma(B^+ \to \rho^+\gamma)/[2\Gamma(B^0 \to \rho^0\gamma)] - 1 = -0.36 \pm 0.27$ in order to test the hypothesis of isospin symmetry. The result is in agreement with the theoretical expectation [2].

Using the measured value of $\mathcal{B}(B \to K^*\gamma)$ [15], we calculate

$$\overline{\mathcal{B}}[B \to (\rho/\omega)\gamma]/\mathcal{B}(B \to K^*\gamma) = 0.024 \pm 0.005. \quad (8)$$

This result is used to determine the ratio of CKM elements $|V_{td}/V_{ts}|$ by means of Equation (2). Following [16], we choose the values $1/\zeta = 1.17 \pm 0.09$, and $\Delta R = 0.1 \pm 0.1$. We find

$$|V_{td}/V_{ts}| = 0.171^{+0.018+0.017}_{-0.021-0.014}, \quad (9)$$

where the first error is experimental and the second is theoretical. This is consistent with the current world average of $|V_{td}/V_{ts}| = 0.201^{+0.008}_{-0.007}$ [17].

Using the measured value of $\mathcal{B}(B^0 \to K^{*0}\gamma)$ [15], we also calculate

$$2 \times \mathcal{B}(B^0 \to \rho^0\gamma)/\mathcal{B}(B^0 \to K^{*0}\gamma) = 0.038^{+0.011}_{-0.010}. \tag{10}$$

By only using these two neutral decay modes, the theoretical interpretation of $|V_{td}/V_{ts}|$ is simplified since the W-annihilation processes present in the $B^+ \to \rho^+\gamma$ channel are avoided. Analogous to Equation (2), taking the same values for $1/\zeta$ and ΔR as above, this result is used to obtain

$$|V_{td}/V_{ts}|_{\rho^0/K^{*0}} = 0.216^{+0.029+0.021}_{-0.031-0.018}, \tag{11}$$

where the first error is experimental and the second is theoretical.

7 SUMMARY

In conclusion, we observe the exclusive $b \to d\gamma$ transitions $B^+ \to \rho^+\gamma$ and $B^0 \to \rho^0\gamma$ and measure the branching fractions $\mathcal{B}(B^+ \to \rho^+\gamma) = (1.06^{+0.35}_{-0.31} \pm 0.09) \times 10^{-6}$ and $\mathcal{B}(B^0 \to \rho^0\gamma) = (0.77^{+0.21}_{-0.19} \pm 0.07) \times 10^{-6}$, where the first error is statistical and the second is systematic. We set an improved 90% C.L. upper limit on the $B^0 \to \omega\gamma$ branching fraction of $\mathcal{B}(B^0 \to \omega\gamma) < 0.84 \times 10^{-6}$. Assuming isospin relations between the three branching fractions, we measure the combined branching fraction $\overline{\mathcal{B}}[B \to (\rho/\omega)\gamma] = (1.01 \pm 0.21 \pm 0.08) \times 10^{-6}$. This result translates into a measurement of the CKM matrix element ratio $|V_{td}/V_{ts}| = 0.171^{+0.018}_{-0.021}(\text{exp.})^{+0.017}_{-0.014}(\text{theor.})$. In addition, we measure the isospin asymmetry $\Gamma(B^+ \to \rho^+\gamma)/[2\Gamma(B^0 \to \rho^0\gamma)] - 1 = -0.36 \pm 0.27$. All these preliminary results are consistent within errors with the SM predictions.

8 ACKNOWLEDGMENTS

We are grateful for the extraordinary contributions of our PEP-II colleagues in achieving the excellent luminosity and machine conditions that have made this work possible. The success of this project also relies critically on the expertise and dedication of the computing organizations that support *BABAR*. The collaborating institutions wish to thank SLAC for its support and the kind hospitality extended to them. This work is supported by the US Department of Energy and National Science Foundation, the Natural Sciences and Engineering Research Council (Canada), Institute of High Energy Physics (China), the Commissariat à l'Energie Atomique and Institut National de Physique Nucléaire et de Physique des Particules (France), the Bundesministerium für Bildung und Forschung and Deutsche Forschungsgemeinschaft (Germany), the Istituto Nazionale di Fisica Nucleare (Italy), the Foundation for Fundamental Research on Matter (The Netherlands), the Research Council of Norway, the Ministry of Science and Technology of the Russian Federation, Ministerio de Educación y Ciencia (Spain), and the Particle Physics and Astronomy Research Council (United Kingdom). Individuals have received support from the Marie-Curie IEF program (European Union) and the A. P. Sloan Foundation.

References

[1] A. Ali and A. Y. Parkhomenko, Eur. Phys. Jour. C **23**, 89 (2002).

[2] A. Ali, E. Lunghi, and A. Y. Parkhomenko, Phys. Lett. B **595**, 323 (2004).

[3] S. W. Bosch and G. Buchalla, Nucl. Phys. B **621**, 459 (2002).

[4] See, for example, S. Bertolini, F. Borzumati, and A. Masiero, Nucl. Phys. B **294**, 321 (1987); H. Baer and M. Brhlik, Phys. Rev. D **55**, 3201 (1997); J. Hewett and J. Wells, Phys. Rev. D **55**, 5549 (1997); M. Carena *et al.*, Phys. Lett. B **499**, 141 (2001).

[5] B. Aubert *et al.* [*BABAR* Collaboration], Phys. Rev. Lett. **94**, 011801 (2005).

[6] T.E. Coan *et al.* [CLEO Collaboration], Phys. Rev. Lett. **84**, 5283 (2000).

[7] D. Mohapatra *et al.* [Belle Collaboration] Phys. Rev. Lett. **96**, 221601 (2006).

[8] B. Aubert *et al.* [*BABAR* Collaboration], Nucl. Instrum. Methods A**479**, 1-116 (2002).

[9] J. Friedman and N. Fisher, Statistics and Computing **9**, 123–143 (1999);
I. Narsky, arXiv:phys/0507143 (2005).

[10] B. Aubert *et al.* [*BABAR* Collaboration], Phys. Rev. Lett. **88**, 101805 (2002).

[11] G.C. Fox and S. Wolfram, Nucl. Phys. B **149**, 413 (1979).

[12] B. Aubert *et al.* [*BABAR* Collaboration], Phys. Rev. Lett. **89**, 201802 (2002).

[13] E.D. Bloom and C.W. Peck, Ann. Rev. Nucl. Part. Sci., **33** 143 (1983).

[14] H. Albrecht *et al.* [ARGUS Collaboration], Z. Phys. C **48**, 543 (1990).

[15] S. Eidelman *et al.* [Particle Data Group], Phys. Lett. B **592**, 1 (2004) and 2005 partial update for edition 2006 (http://pdg.lbl.gov/).

[16] P. Ball and R. Zwicky, JHEP **0604**, 046 (2006).

[17] J. Charles *et al.* [CKMfitter Group], Eur. Phys. Jour. C **41**, 1 (2005) and online update for FPCP 2006 (http://ckmfitter.in2p3.fr/).

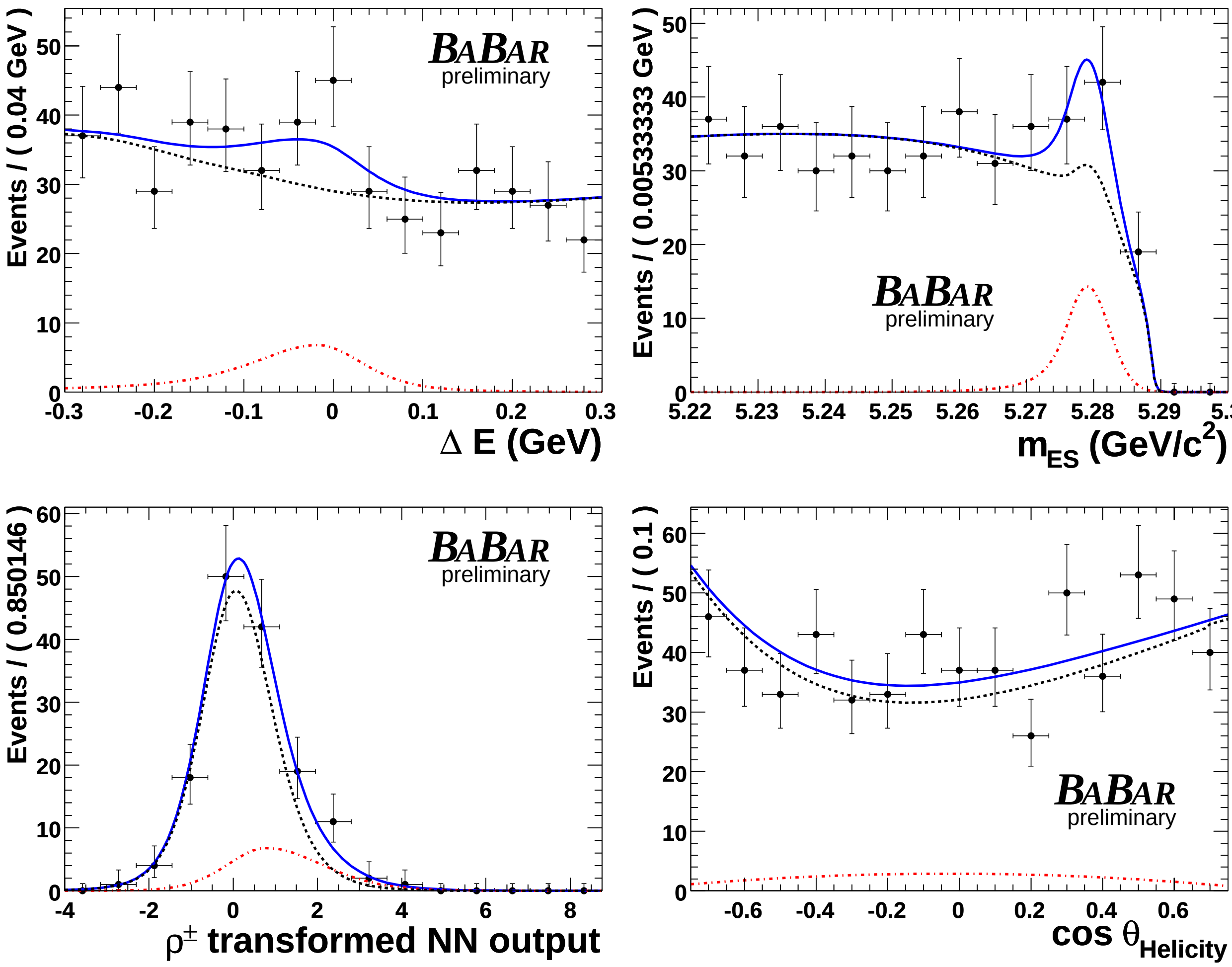

Figure 2: Projections of the fits to the $B^+ \to \rho^+\gamma$ sample in the discriminating variables ΔE (upper left), $m_{\rm ES}$ (upper right), $\mathcal{NN}$ (lower left), and $\cos\theta_H$ (lower right). The points are data, the solid line is the total PDF and the dark dashed (light dot-dashed) line is the background (signal) only PDF. The selections applied, unless the variable is projected, are: $-0.15 < \Delta E < 0.05$ GeV, $5.275 < m_{\rm ES} < 5.285$ GeV/c^2, and $\mathcal{NN} > 0.0$.

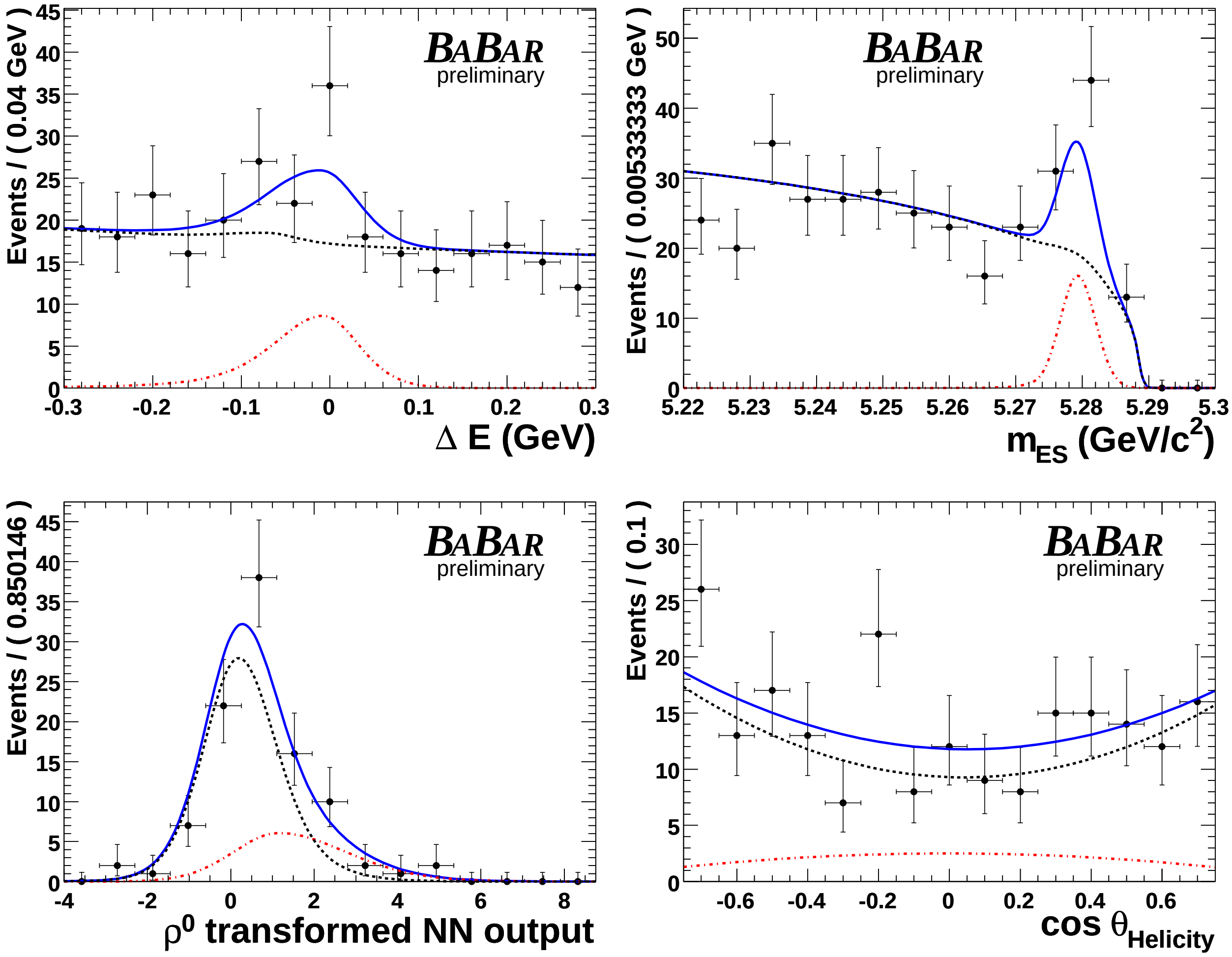

Figure 3: Projections of the fits to the $B^0 \to \rho^0\gamma$ sample in the discriminating variables ΔE (upper left), $m_{\rm ES}$ (upper right), $\mathcal{NN}$ (lower left), and $\cos\theta_H$ (lower right). The points are data, the solid line is the total PDF and the dark dashed (light dot-dashed) line is the background (signal) only PDF. The selections applied, unless the variable is projected, are: $-0.15 < \Delta E < 0.05$ GeV, $5.275 < m_{\rm ES} < 5.285$ GeV/c^2, and $\mathcal{NN} > 0.0$.

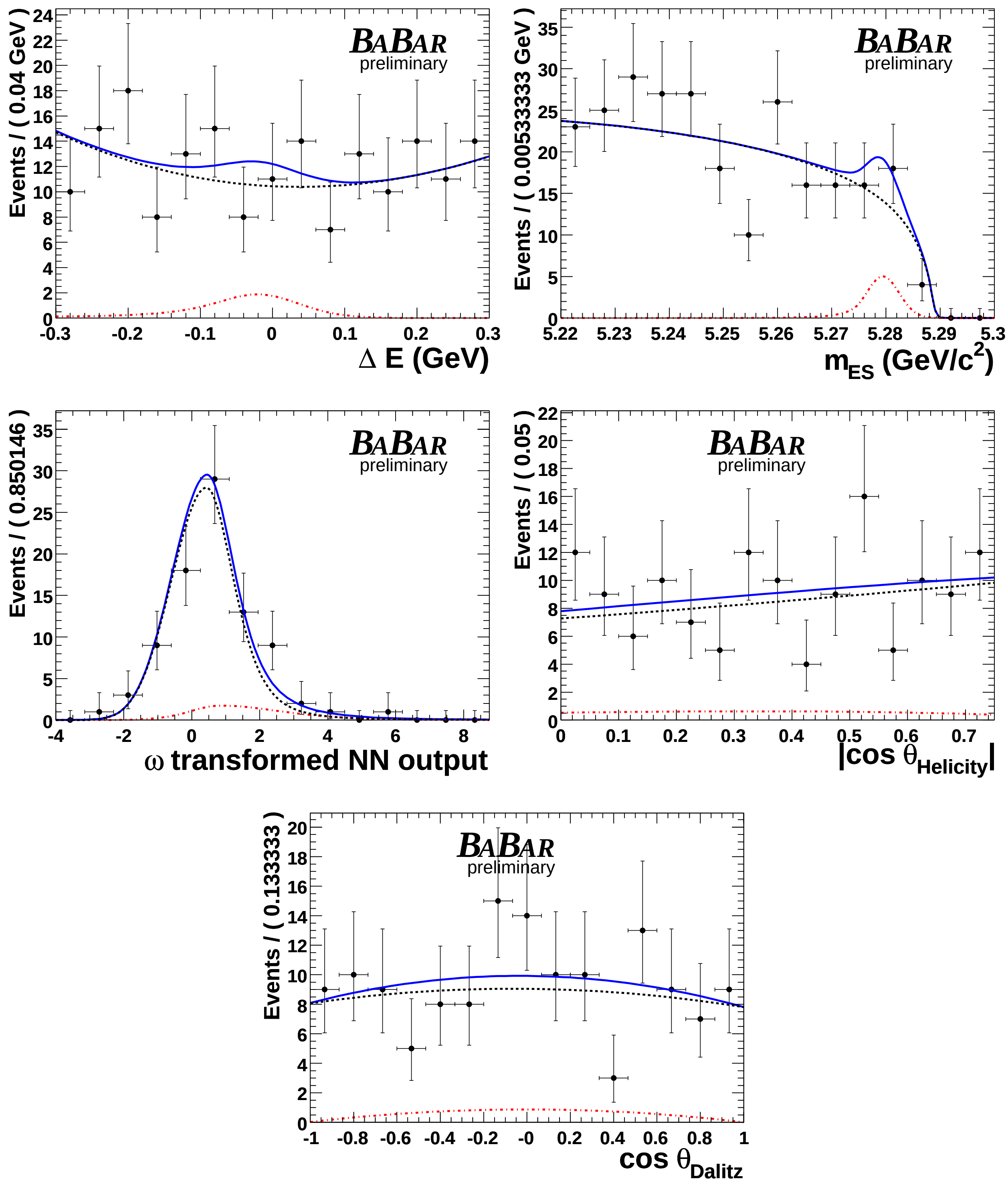

Figure 4: Projections of the fits to the $B^0 \to \omega\gamma$ sample in the discriminating variables ΔE (upper left), $m_{\rm ES}$ (upper right), $\mathcal{NN}$ (middle left), $\cos\theta_H$ (middle right), and $\cos\theta_D$ (bottom). The points are data, the solid line is the total PDF and the dark dashed (light dot-dashed) line is the background (signal) only PDF. The selections applied, unless the variable is projected, are: $-0.15 < \Delta E < 0.05$ GeV, $5.275 < m_{\rm ES} < 5.285$ GeV/c^2, and $\mathcal{NN} > 0.0$.